Self-Assembly of Molecular Dumbbells into Organized Bundles with Tunable Size

Myongsoo Lee,*[a] Yang-Seung Jeong,[a] Byoung-Ki Cho,[a] Nam-Keun Oh,[b] and Wang-Cheol Zin[b]

Abstract: Dumbbell-shaped molecules consisting of three biphenyls connected through vinyl linkages as a conjugated rod segment and aliphatic polyether dendritic wedges with different cross-sections (i.e., dibranch (**1**), tetrabranch (**2**) and hexabranch (**3**)) were synthesized and characterized. The molecular dumbbells self-assemble into discrete bundles that organize into three-dimensional superlattices. Molecule **1**, based on a dibranched dendritic wedge, organizes into primitive monoclinic-crystalline and body-centered, tetragonal liquid crystalline structures, while molecules **2** and **3**, based on tetra- and hexabranched dendritic wedges, respectively, form only body-centered, tetragonal liquid crystalline structures. X-ray diffraction experiments and density measurements showed that the rod-bundle cross-sectional area decreases with increasing cross-section of the dendritic wedges. The influences of supramolecular structure on the bulk-state optical properties were investigated by measuring the UV/Vis absorption and steady state fluorescence spectroscopies. As the cross-section of the dendritic wedge of the molecule increases, the absorption and emission maxima shift to higher energy. This can be attributed to a quantum size effect of the three-dimensionally confined nanostructure.

Keywords: dendrimers · molecular dumbbells · nanostructures · quantum size effect · self-assembly

Introduction

The design and construction of molecular materials assembled in organized structures with desirable functions and properties is an area of great interest. The development of such molecular materials requires the rational design of molecular components that are programmed to assemble through noncovalent intermolecular forces, such as dipolar interactions, hydrogen bonding, shape-conforming dispersive interactions, and repulsive forces between dissimilar parts of the molecule.[1, 2] These interactions lead to molecular aggregates that are regular in shape and size, and have some properties that are unlike either their molecular components or the bulk properties of similar materials. For example, rod building blocks can generate organized objects of nanoscale dimensions through the combination of shape complementarity and the repulsive interactions of rigid and flexible parts.[3] Previous experiments from our laboratory have demonstrated that the self-assembled structure based on rod building blocks can be manipulated through the attachment of flexible parts of different lengths to their ends.[4] Depending on the relative length of the flexible segments, these blocks self-assemble into infinitely long cylinders or dissimilar cylinders that organize into two-dimensional, hexagonal or three-dimensional, tetragonal superlattices.[5] Honeycomb supramolecular structures assembled from elongated rods and able to self-organize into a three-dimensional hexagonal superlattice, have also been reported.[6]

Supramolecular structure has a strong impact on the photophysical properties of optically active materials. As a result, a number of self-assembling materials have been developed from conjugated rod building blocks in order to establish the supramolecular structure–property relationship.[7] A recent publication from our laboratory described how a strategy to manipulate the optically active supramolecular structure from one-dimensional to three-dimensional superlattices could be accessible by incorporation of the conjugated rod into a rod–coil architecture.[5b] This experiment confirmed that the shape of the supramolecular structure assembled from optically active rod building blocks has a strong influence on the photophysical properties of supramolecular materials. However, despite the accepted fact that the size of discrete nanostructures significantly alters the photophysical properties of optically active materials, no reports of a general method for controlling the size of conjugated rod aggregate have appeared.

[a] Prof. M. Lee, Y.-S. Jeong, B.-K. Chon
Department of Chemistry, Yonsei University
Shinchon 134, Seoul 120-749 (Korea)
Fax: (+82) 2-364-7050
E-mail: mslee@yonsei.ac.kr

[b] N.-K. Oh, Prof. W.-C. Zin
Department of Materials Science and Engineering
Pohang University of Science and Technology
Pohang 790-784 (Korea)

  0947-6539/02/0804-0876 $ 17.50+.50/0

A strategy to manipulate the size of the discrete nanostructures assembled from conjugated rod building blocks may be accessible by attaching chemically dissimilar, flexible dendritic wedges to their ends. As the cross-sectional area of the dendritic wedge of the molecule increases (while maintaining the anisotropic order of the rod building blocks) greater steric repulsion between adjacent dendritic wedges could possibly cause a reduction in the number of assembled rod building blocks per aggregate in order to relieve the repulsive forces. This implies that the cross-section of the dendritic building blocks in a molecule has an impact on the size of aggregate assembled from the rod blocks. With this in mind, we have synthesized dumbbell-shaped molecules that are based on a conjugated rod block and chemically dissimilar, flexible dendritic wedges of different cross-sectional area.

In this paper, we report the synthesis of molecular dumbbells consisting of three biphenyls, connected through vinyl linkages as a conjugated rod segment, and aliphatic polyether dendritic wedges with different cross-sections, that is, dibranch (**1**), tetrabranch (**2**), and hexabranch (**3**) (Scheme 1). Since the dendritic building blocks are all based on nearly identical molecular weights, the shape and size of the aggregate may mainly be attributed to the variation in the cross-sectional area of the dendritic wedge.

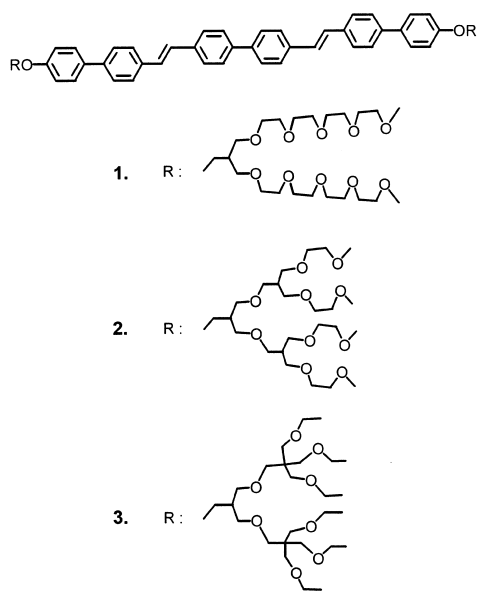

Scheme 1. Chemical structure of dumbbell-shaped molecules **1**–**3**.

Results and Discussion

The synthesis of these molecules was performed in a stepwise fashion starting with a convergent route to the polyether dendron by using etherification chemistry[8] and continuing with a Wittig–Horner reaction[9] to generate the rod building block (Schemes 2 and 3). All of the final products were characterized by 1H and 13C NMR spectroscopy, elemental analysis, and gel-permeation chromatography (GPC), and shown to be in full agreement with the structures presented. It should be noted that the *trans* selectivity of the Wittig–Horner reaction in its final step is sufficiently high to generate all-*trans* isomers **1**–**3** within the limits of NMR detection.

The thermotropic phase behavior of **1**–**3** was investigated by a combination of techniques consisting of differential scanning calorimetry (DSC), thermal, optical, polarized microscopy, and X-ray scattering experiments. Figure 1 presents the DSC heating and cooling traces of **1**–**3**. All of the molecules show an ordered bulk-state structure. The transition temperatures and corresponding enthalpy changes determined from the DSC scans are summarized in Table 1. As can be observed from Figure 1 and Table 1, molecule **1**, based on a dibranched dendritic wedge, has a crystalline melting transition at 138 °C, followed by a liquid crystalline phase that transforms into an isotropic liquid at 233 °C. On slow cooing from the isotropic liquid, the formation of unique domains, which grow in four directions and coalesce into a mosaic texture, could easily be observed under a polarized optical microscope. This suggests the presence of a tetragonal liquid crystalline phase at a higher temperature (Figure 2).[5a] Small-angle X-ray scattering (SAXS) in the solid state revealed a number of well-resolved reflections; this indicated the existence of a highly ordered nanoscopic structure (Figure 3a). These reflections can be indexed as a three-dimensional primitive monoclinic structure with a characteristic angle of 69° and lattice parameters $a = 5.8$ nm, $b = 4.9$ nm, and $c = 6.2$ nm (Table 3).[10] As shown in Figure 4a, the wide-angle X-ray scattering revealed a reflection at a q-spacing of about 4.42 Å, which is due to crystal packing of the rod segments within the aromatic domains. To better understand the packing arrangement of the rod building blocks within the supramolecular unit, it is desirable to calculate the number of molecules in each aggregate. The lattice constants determined from SAXS patterns and measured densities suggest that the average number (n) of molecules in each supramolecular aggregate is approximately 73 (Table 2). The tendency of the rod building blocks to be arranged into anisotropic crystalline order along their axes seems to generate nonspherical aggregates, which are responsible for the formation of the unusual three-dimensional monoclinic superlattice. In addition, this monoclinic nature with three characteristic dimensions suggests that the aggregation of 73 rod segments in each aggregate generates the rod-bundles with cross-sections that are more rectangular than circular in shape.

In the melt state, the SAXS pattern shows a sharp, high intensity reflection at a low angle together with a number of sharp reflections of low intensity at higher angles (Figure 3b). Similarly to the result from our laboratory described previously,[6] these reflections can be indexed as a three-dimensional, body-centered, tetragonal lattice with $c/a = 0.92$. At a wide-angle, only a diffuse halo remains as evidence of the lack of any positional long-range order other than the three-dimensional tetragonal packing of supramolecular units (Figure 4b). These results, together with optical microscopic observations, indicate that **1** has a three-dimensional, body-centered, tetragonal liquid crystalline phase with lattice constants of $a = 6.5$ nm and $c = 6.0$ nm.

Molecules **2** and **3**, based on tetra- and hexabranched dendritic wedges, respectively, have birefringent waxy states

  0947-6539/02/0804-0877 $ 17.50+.50/0

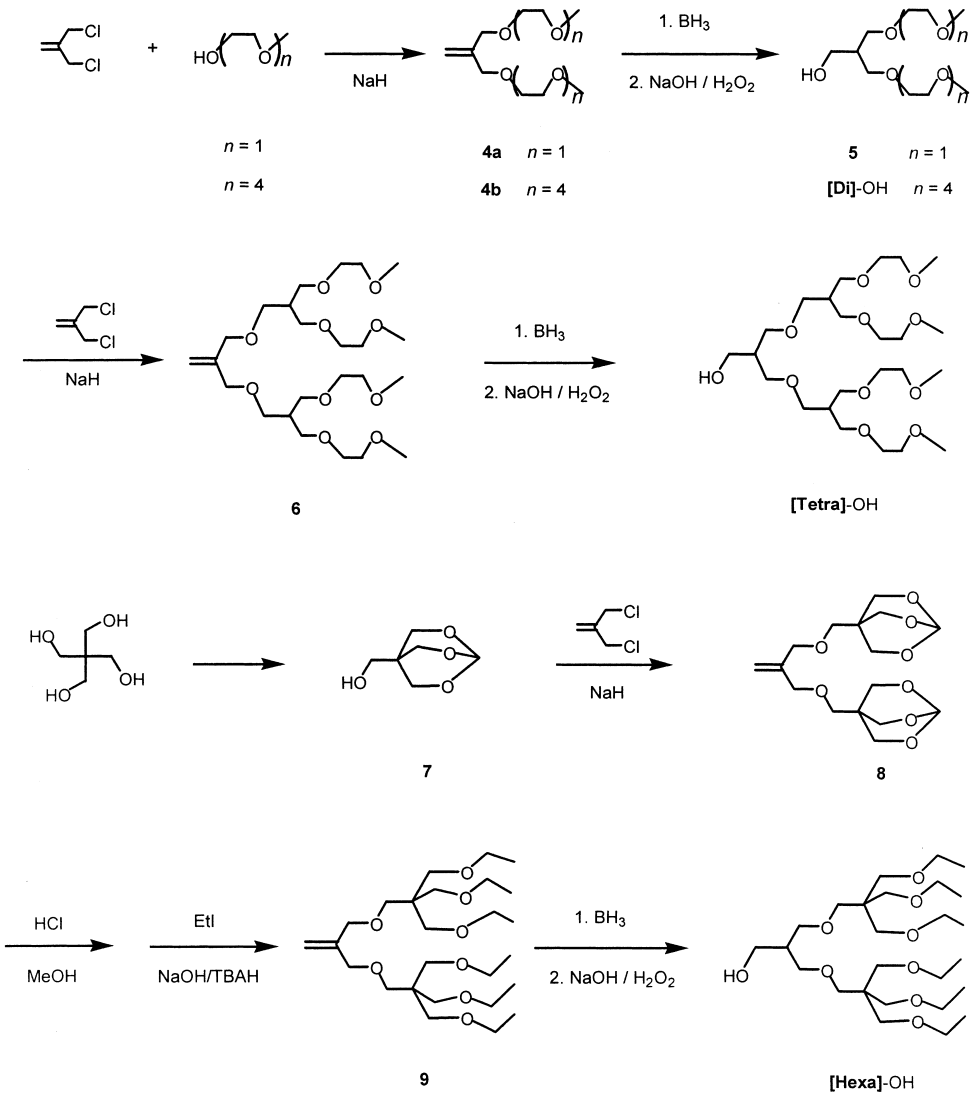

Scheme 2. Synthesis of dendritic building blocks **[Di]**-OH, **[Tetra]**-OH and **[Hexa]**-OH.

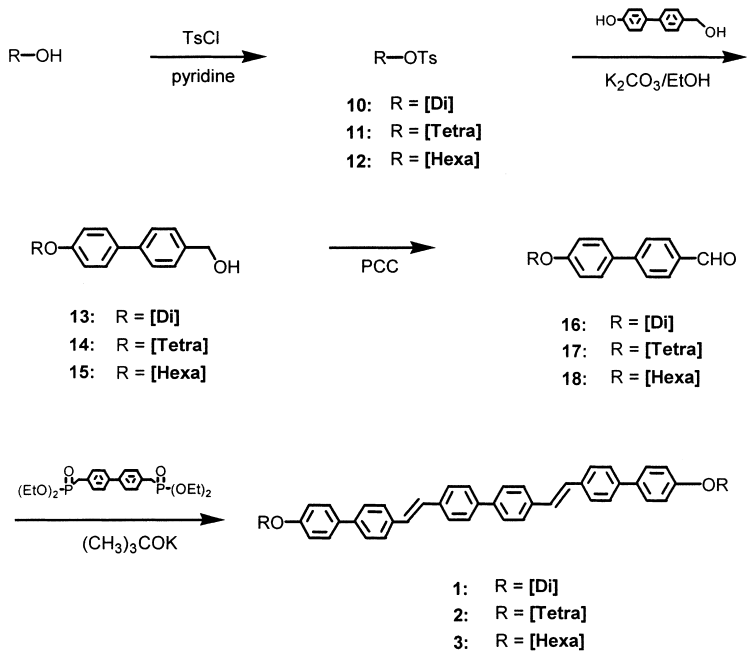

Scheme 3. Synthesis of molecular dumbbells **1**–**3**.

that are retained up to the isotropization temperature (201 °C and 173 °C for **2** and **3**, respectively; Table 1). The SAXS patterns of these molecules, recorded at 30 °C, are shown in Figure 3c and d, and correspond to the three-dimensional, body-centered, tetragonal superlattices with $c/a = 0.93$ and 0.92 for **2** and **3**, respectively. The observed *d*-spacings and the lattice constants are summarized in Table 2. While the WAXS patterns of these molecules show a broad halo centered at approximately 4.6 Å, which is similar to that of the liquid crystalline phase of **1** and indicates a liquid crystalline order (Figure 4c and d); the lack of crystallinity in the rod building blocks of these molecules is most likely due to confinement between dendritic wedges with larger cross-sectional area. Considering that the three-dimensional tetragonal structure consists of discrete supramolecular structures, the inner core consists of a rod-bundle that is encapsulated by flexible dendritic wedges; this gives rise to the formation of nonspherical oblate aggregates. These aggregates self-organize into a three-dimensional, body-centered, tetragonal superlattice. The lattice constants and measured densities suggest that the average number (n) of molecules in each supramolecular aggregate is approximately 47 for **2** and 39 for **3** (Table 2). The aggregation of the rod segments into a micelle can be estimated to generate a rod-bundle with a relatively flat cylindrical shape. The shape of the aromatic domain seems to be responsible for the formation of oblate aggregates, which organize into a three-dimensional, tetragonal superlattice.

Figure 5 illustrates the mechanism for self-assembly of the molecular dumbbells

0947-6539/02/0804-0878 $ 17.50+.50/0 *Chem. Eur. J.* **2002**, *8*, No. 4

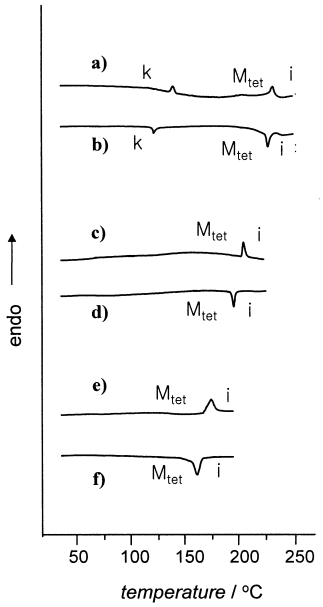

Figure 1. DSC traces ($10\,^{\circ}C\,min^{-1}$) recorded during a) the heating and b) the cooling scan of **1**; c) the heating and d) the cooling scan of **2**; e) the heating and f) the cooling scan of **3**.

Figure 2. Representative optical polarized micrograph ($100\times$) of texture exhibited by a body-centered tetragonal micellar mesophase of **1** at the transition from the isotropic liquid state at 220 °C.

responsible for the generation of the three-dimensional superlattices, the lattice dimensions, the number (n) of molecules forming the rod-bundle, and their sizes (A) in cross-sectional area. The results from Table 2 and Figure 5 indicate that the number of molecules per bundle decreases systematically with increasing cross-section of the dendritic wedge. Consequently, the size of the rod-bundle in cross-

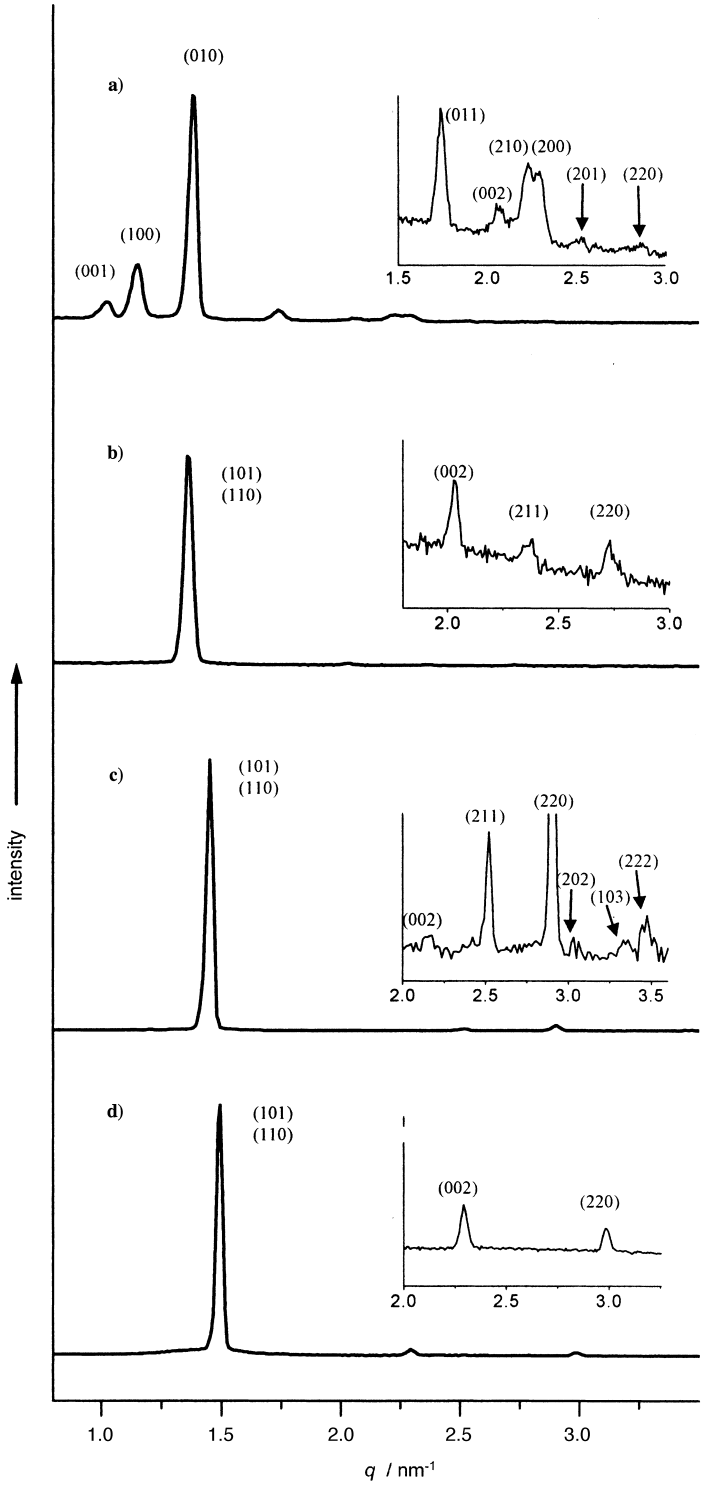

Figure 3. Small-angle X-ray diffraction patterns of a) **1** at 60 °C, b) **1** at 150 °C, c) **2** at 30 °C, and d) **3** at 30 °C.

Table 1. Thermal transitions of molecular dumbbells **1**–**3** (data from second heating and first cooling scans).[a]

molecules	$\frac{M_w}{M_n}$[b]	phase transition temperatures [°C] with corresponding enthalpy changes in brackets [kJ mol^{-1}] heating	cooling
1	1.04	k 138.2 (0.34) M_{tet} 233.2(0.70) i	i 224.9 (0.77) M_{tet} 121.5 (0.27) k
2	1.05	M_{tet} 201.4 (0.68) i	i 189.1 (0.70) M_{tet}
3	1.04	M_{tet} 172.5 (1.64) i	i 163.5 (1.61) M_{tet}

[a] k = crystalline, M_{tet} = body-centered tetragonal mesophase, i = isotropic. [b] Determined from GPC data.

  0947-6539/02/0804-0879 $ 17.50+.50/0

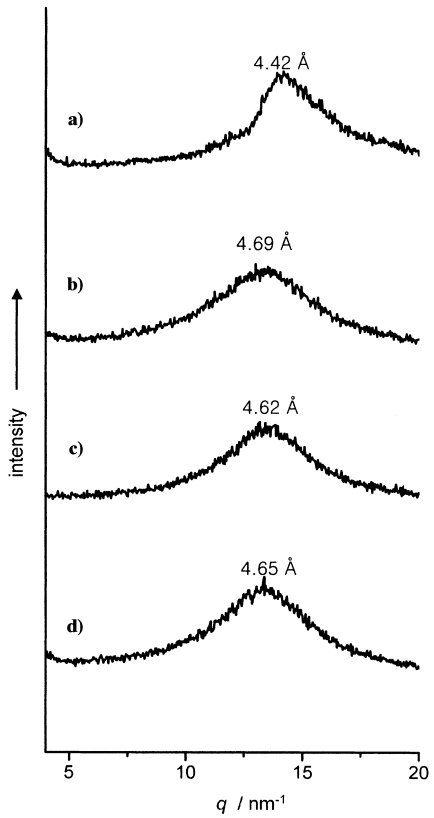

Figure 4. Wide-angle X-ray diffraction patterns of a) **1** at 30 °C, b) **1** at 150 °C, c) **2** at 30 °C and d) **3** at 30 °C.

sectional area decreases in nanoscale dimension from 17.0 to 11.5 to 9.6 nm2 for **1**, **2**, and **3**, respectively. This result demonstrates the capability of manipulating the size of the bundles based on the same rod building block by attaching flexible dendritic wedges of different cross-sectional area, but similar molecular weight, to their ends. The variation of rod-bundle size in cross-section can be rationalized by considering both the steric repulsion between the bulky dendritic wedges and the nanophase separation between the dissimilar parts of the molecule.[4, 10] Anisotropic ordering of the rod building blocks in the molecule should exclude chemically dissimilar dendritic segments. Because dendritic wedges have a large cross-section, they will encounter strong repulsive forces when trying to accommodate the density of the ordered rod building blocks. These repulsive forces could balance the favorable aggregation of rod building blocks and generate the finite aggregation of dumbbell-shaped molecules. As the cross-sectional area of the dendritic wedges increases, so do the repulsive forces between them. Consequently, this increase in steric repulsion could give rise to smaller aggregates that allow more space for the dendritic building blocks to adopt a less strained conformation.

Table 3. Small angle X-ray diffraction data for the primitive monoclinic structure of **1** measured at 60 °C.[a]

h k l	q_{calcd} [nm^{-1}]	q_{obsd} [nm^{-1}]
0 0 1	1.018	1.018
1 0 0	*1.153*	*1.153*
0 1 0	1.381	1.381
0 1 1	1.716	1.737
0 0 2	2.036	2.050
2 1 0	2.221	2.228
2 0 0	2.307	2.285
2 0 1	2.520	2.529
2 2 0	2.897	2.858

[a] q_{calcd} and q_{obsd} are the scattering vectors of the calculated and observed reflections for the primitive monoclinic structure with lattice parameters $a = 5.8$ nm, b 4.9 nm, c 6.2 nm ($\gamma = 69°$).

The effects of supramolecular structure on the bulk-state optical properties were investigated by measuring the UV/Vis absorption and steady state fluorescence spectroscopies. Figure 6 shows the absorption and fluorescence spectra of **1**, **2**, and **3**. The bulk state absorption spectra of the molecules exhibit an intense transition with a maximum at 378, 374, or 368 nm for **1**–**3**, respectively, resulting from the conjugated rod block. The bulk-state fluorescence spectra show a strong maximum between 460 and 480 nm, which does not appear in the solution spectra; this suggests that the band comes from π-stacking of the rod building blocks. Interestingly, the absorption maxima and absorption edges in the spectra of **1**–**3** progressively shift to higher energy, as the cross-section of the dendritic wedge of the molecule increases. In addition, the emission maxima appear to be 479, 469, and 462 nm for **1**–**3**, respectively; this indicates that an increased cross-section of the dendritic wedge also causes a blue shift of the emission maximum. These results could be attributed to quantum size effect of the three-dimensionally confined nanostructures as evidenced by the results shown in Table 2 and Figure 5. The absorption and emission maxima and the absorption edge in semi-conducting nanoparticles have been reported to be blue shifted with decreasing particle size, especially in the range of 1 to 10 nm in diameter.[11] This trend may also arise from the slightly different intermolecular interactions between adjacent conjugated rods that occur with the variation in the cross-section of the dendritic wedge.[12] However, the size effects and intermolecular interactions seem to be cooperative, and their contribution could be equally important in the photophysical properties of the supramolecular materials. The

Table 2. Characterization of molecular dumbbells by small angle X-ray scattering.

molecule	T [°C]	density (g cm^{-3}) r[a]	r_{rod}[b]	n	d_{110} [nm]	d_{100} [nm]	d_{010} [nm]	d_{001} [nm]	lattice constant a [nm]	b [nm]	c [nm]	g [°]	A [nm^2][e]
1	25	1.083	1.287	73[C]		5.4	4.6	6.2	5.8	4.9	6.2	69	17.0
	150				4.6				6.5	6.5	6.0		
2	25	1.062	1.223	47[d]	4.4				6.2	6.2	5.8		11.5
3	25	1.020	1.201	39[d]	4.2				5.9	5.9	5.5		9.6

[a] Molecular density. [b] Density of rod segment. [c] Number of molecules in a monoclinic unit cell $n = abc \cdot \sin(\gamma) N_A \rho / M$ (N_A = Avogadro's number, ρ = molecular density, M = molecular weight). [d] Number of molecules in a micelle $n = a^2 c N_A \rho / 2M$ (ρ = molecular density). [e] Cross-sectional area of a rod bundle $A = nM_{rod}/N_A \rho_{rod} h_{rod}$ (M_{rod} = molecular weight of rod segment, h_{rod} = length of rod segment).

0947-6539/02/0804-0880 $ 17.50+.50/0 *Chem. Eur. J.* **2002**, *8*, No. 4

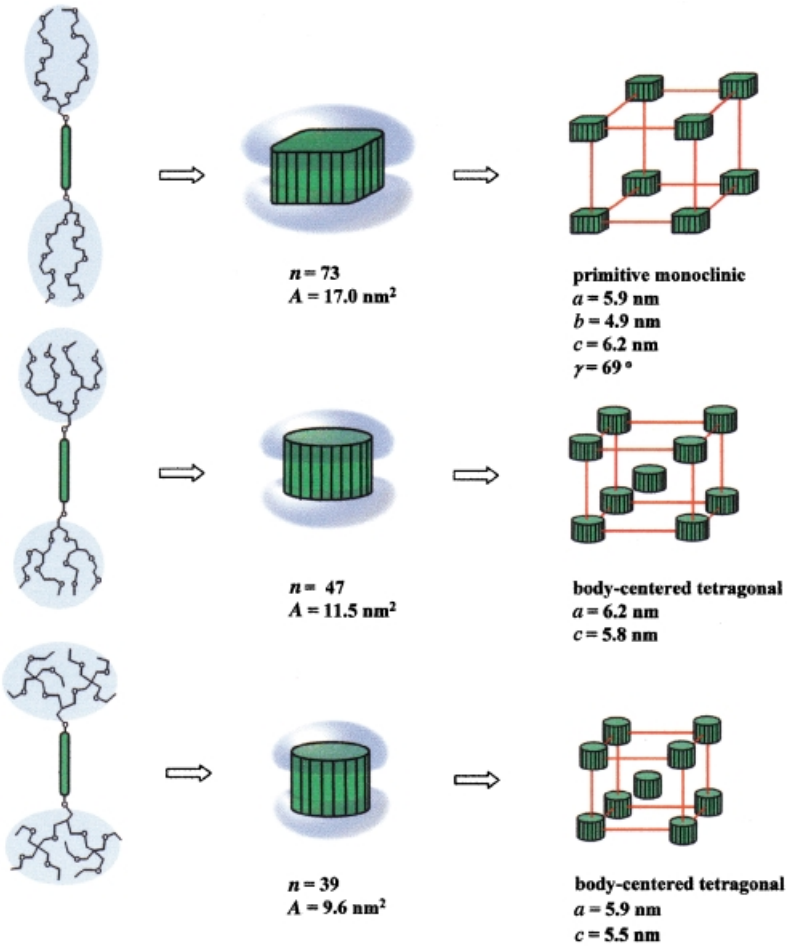

Figure 5. Structural analysis of the supramolecular bundles assembled from molecular dumbbells **1**–**3**; n is the number of molecules per aggregate and A is the cross sectional area of the rod-bundle.

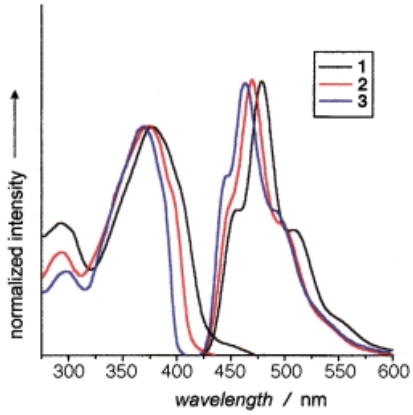

Figure 6. UV/Vis absorption (left) and fluorescence (right) spectra of **1**–**3** in the bulk state.

definitive feature of the driving forces responsible for the variation in optical properties depending on the bundle size is the subject of ongoing investigations.

Conclusion

Molecular dumbbells consisting of a conjugated rod and dendritic wedges have been synthesized and characterized, and their self-assembling behavior has been investigated. The molecular dumbbells, which have different dendritic wedges, self-assemble into discrete bundles of tunable size that organize into three-dimensional superlattices. With increasing cross-section of the dendritic wedge, the number of molecules per aggregate decreases, and, as a consequence, the rod-bundle cross-section decreases. Therefore, the size control of the bundles assembled from the rod building blocks is determined by the cross-section of the flexible segment attached to the rod ends. Spectroscopic studies of these molecules demonstrate that the size of the optically active rod bundle has an influence on the photophysical properties of the conjugated rods, and consequently our approach to controlling the size of the nanostructure by synthesis provides a strategy for controlling supramolecular material characteristics.

Experimental Section

Materials: 4-(Hydroxymethyl)biphenyl-4′-ol (99%), toluene-*p*-sulfonyl chloride (98%), NaH (60%), and ethyl iodide (99%) from Tokyo Kasei were used as received. Ethylene glycol momomethyl ether (98%), pentaerythritol (99%), and tetrabutylammonium hydrogen sulfate (TBAH, 97%) from Aldrich and other conventional reagents were used as received.

Techniques: ^{1}H and ^{13}C NMR spectra were recorded as solutions in $CDCl_3$ on a Bruker AM 250 spectrometer. The purity of the products was checked by thin layer chromatography (TLC; Merck, silica gel 60). A Perkin Elmer DSC-7 differential scanning calorimeter, equipped with 1020 thermal analysis controller, was used to determine the thermal transitions, which were reported as the maxima and minima of their endothermic or exothermic peaks. In all cases, the heating and cooling rates were 10 °C min − 1. A Nikon Optiphot 2-pol optical polarized microscope (magnification: 100×), equipped with a Mettler FP 82 hot-stage and a Mettler FP 90 central processor, was used to observe the thermal transitions and to analyze the anisotropic texture. Microanalyses were performed with a Perkin Elmer 240 elemental analyzer at the Organic Chemistry Research Center. X-ray scattering measurements were performed in transmission mode with synchrotron radiation at the 3C2 X-ray beam line at the Pohang Accelerator Laboratory, Korea. Molecular weight distributions (M_w/M_n) were determined by gel permeation chromatography (GPC) with a Waters R401 instrument equipped with Stragel HR 3, 4, and 4E columns, M7725i manual injector, column heating chamber, and 2010 Millennium data station. Measurements were made by using a UV detector and $CHCl_3$ as solvent (1.0 mL min − 1). The molecular density (ρ) measurements were performed in aqueous sodium chloride solution at 25 °C. Optical absorption spectra were obtained from a Shimadzu 1601 UV spectrophotometer. The fluorescence spectra were obtained from a Hitachi F-4500 fluorescence spectrophotometer.

Synthesis: A general outline of the synthetic procedure is shown in Schemes 2 and 3. The synthesis of the polyether dendritic building blocks was performed according to the similar procedures reported previously.[8]

Synthesis of 4a, 4b and 6c: These compounds were synthesized according to the same procedure; a representative example is described for **4a**. Dry NaH (3.2 g, 80 mmol), methallyl dichloride (3.8 g, 30 mmol), and freshly distilled dry THF (50 mL) were placed in a dry round bottomed flask under N_2. Ethylene glycol monomethyl ether (5.5 g, 72 mmol) was added dropwise to this mixture at room temperature, and the mixture was stirred at ~65 °C for 12 h. After cooling to room temperature, the reaction mixture was quenched with water and extracted with diethyl ether. The organic layer was dried over anhydrous $MgSO_4$, the solvent was removed in a rotary evaporator, and the crude product was purified by column chromatography (silica gel) with ethyl acetate as eluent to give a colorless liquid. **4a**: yield: 5.1 g (83.9%); 1H NMR (250 MHz, $CDCl_3$): $\delta = 5.18$ (s, 2H; CH_2C), 4.02 (s, 4H; $CH_2C(CH_2O)_2$), 3.53 (t, $J = 3.5$ Hz, 8H; OCH_2), 3.36 (s, 6H; OCH_3). **4b**: yield: 86.7%; 1H NMR (250 MHz, $CDCl_3$): $\delta =$ 5.18 (s, 2H; CH_2C), 4.01 (s, 4H; $CH_2C(CH_2O)_2$), 3.70–3.58 (m, $J = 3.5$ Hz, 32H; OCH_2), 3.37 (s, 6H; OCH_3). **6c**: yield: 83.9%; 1H NMR (250 MHz, $CDCl_3$): $\delta = 5.18$ (s, 2H; CH_2C), 4.02 (s, 4H; $CH_2C(CH_2O)_2$) 3.62–3.41 (m, 28H; OCH_2), 3.37 (s, 12H; OCH_3), 2.22–2.04 (m, 2H; $CH(OCH_2)_2$).

Synthesis of 8: Dry NaH (3.2 g, 80 mmol), methallyl dichloride (3.2 g, 25.6 mmol), and freshly distilled dry THF (50 mL) were placed in a dry round bottomed flask under N_2. Compound **7** (7.5 g, 51.2 mmol) was added dropwise to this mixture at room temperature. The mixture was stirred at room temperature for 15 min and at 65 °C for 12 h. After cooling to room temperature, the reaction mixture was quenched with water (5 mL), and the THF was removed in a rotary evaporator. The crude mixture was washed with water (2 × 20 mL) and filtered to afford a yellow solid. Dried crude product could be separated by column chromatography (silica gel) with CH_2Cl_2 as eluent. Yield: 8.2 g (93.2%); 1H NMR (250 MHz, $CDCl_3$): $\delta = 5.50$ (s, 2H; $CH(CH_3)_3$), 5.18 (s, 2H; CH_2C), 4.02 (s, 4H; $CH_2C(CH_2O)_2$), 3.45–3.37 (m, 16H; OCH_2).

Synthesis of 9: Compound **8** (5.7 g, 16.6 mmol) was mixed with of methanol (50 mL), containing HCl (1 mL, 12 M). MeOH was distilled off very slowly over 3 h. After cooling the mixture to room temperature, methanol was removed by rotary evaporation, and yellow crude product was obtained. This mixture was used directly for next step with aqueous NaOH (50% *w*/*w*, 20 mL), tetrabutylammonium hydrogen sulfate (0.56 g, 1.7 mmol), and ethyl iodide (24.3 g, 156 mL). The reaction mixture was stirred at 75 °C for 72 h. After cooling to room temperature, the reaction mixture was poured into ice water and extracted with diethyl ether. The organic layer was dried over anhydrous $MgSO_4$, the solvent was removed in a rotary evaporator, and the crude product was purified by column chromatography (silica gel) with diethyl ether as eluent to give a colorless liquid. Yield: 7.51 g (70.3%); 1H NMR (250 MHz, $CDCl_3$): $\delta = 5.18$ (s, 2H; CH_2C), 4.02 (s, 4H; $CH_2C(CH_2O)_2$), 3.37 (m, 28H; OCH_2), 1.15–1.10 (m, 18H; OCH_2CH_3).

Synthesis of 5, [Di]-OH, [Tetra]-OH and [Hexa]-OH: Compounds were synthesized by the same procedure. A representative example is described for **[Tetra]**-OH. Freshly distilled dry THF (5 mL) and **6** (4.9 g, 9.9 mmol) were placed in a dry round bottomed flask under N_2 and cooled to 0 °C in a ice bath. A solution of BH_3 (1 M) in THF (11 mL) was added slowly to this mixture, which was then stirred at 0 °C for 2 h. The reaction mixture was quenched with a solution of NaOH in water (3 M, 4 mL) and allowed to stir for 15 min. This was followed by addition of an H_2O_2 aqueous solution of (30%, 4 mL), and the mixture was stirred at room temperature for 30 min. The reaction mixture was saturated with K_2CO_3 and extracted with diethyl ether. The organic layer was dried over anhydrous $MgSO_4$, the solvent was removed in a rotary evaporator, and the crude product was purified by column chromatography (silica gel) with ethyl acetate as eluent to afford a colorless liquid. **5**: yield: 90.1%; 1H NMR (250 MHz, $CDCl_3$): $\delta = 3.76$–3.50 (m, 14H; OCH_2), 3.37 (s, 6H; OCH_3), 2.03 (m, $J = 12.5$Hz, 1H; $CH(OCH_2)_2$). **[Di]**-OH: yield: 75.5%; 1H NMR (250 MHz, $CDCl_3$): $\delta =$ 3.62–3.41 (m, 38; OCH_2), 3.37 (s, 6H; OCH_3), 2.04 (m, 1H; $CH(OCH_2)_2$). **[Tetra]**-OH: yield: 4.7 g (90.3%); 1H NMR (250 MHz, $CDCl_3$): $\delta = 3.62$–3.41 (m, 34H; OCH_2), 3.37 (s, 12H; OCH_3), 2.22–2.04 (m, 3H; $CH(OCH_2)_2$). **[Hexa]**-OH: yield: 72.1%; 1H NMR (250 MHz, $CDCl_3$): $\delta = 3.62$–3.41 (t, 34H; OCH_2), 2.22–2.04 (m, 1H; $CH(OCH_2)_2$), 1.15 (t, $J = 6.2$ Hz, 18; OCH_2CH_3).

Synthesis of 10, 11, and 12: Compounds were synthesized by using the same procedure. A representative example is described for **11**. **[Tetra]**-OH (10.6 g, 20.6 mmol) and TsCl (8.1 g, 41.1 mmol) were dissolved of dry dichloromethane (80 mL), and pyridine (4.4 g, 61.8 mmol) was then added under nitrogen. The reaction mixture was stirred at 25 °C under nitrogen for 5 h. The resulting solution was washed with water, and the dichloromethane solution was dried over anhydrous magnesium sulfate and filtered. The solvent was removed in a rotary evaporator, and the crude product was purified by column chromatography (silica gel) with methylene chloride as eluent to give a colorless liquid. **10**: yield: 75.3%; 1H NMR (250 MHz, $CDCl_3$): $\delta = 7.79$ (d, $J = 8.3$ Hz, 2Ar-H; *o* to SO_3), 7.36 (d, $J = 8.3$ Hz, 2Ar-H; *m* to SO_3), 4.08 (d, $J = 5.5$ Hz, 2H; SO_3CH_2), 3.56–3.43 (m, 36H; OCH_2), 3.37 (s, 12H, OCH_3), 2.44 (s, 3H; phenyl CH_3), 2.27–2.18 (m, 1H; $OCH(OCH_2)_2$). **11**: yield: 12.5g (91.2%); 1H NMR (250 MHz, $CDCl_3$): $\delta =$ 7.79 (d, $J = 8.3$ Hz, 2Ar-H; *o* to SO_3), 7.36 (d, $J = 8.3$ Hz, 2Ar-H; *m* to SO_3), 4.08 (d, $J = 5.5$ Hz, 2H; SO_3CH_2), 3.56–3.43 (m, 32H; OCH_2), 3.37 (s, 12H, OCH_3), 2.44 (s, 3H; phenyl CH_3), 2.27–2.18 (m, 3H; $OCH(OCH_2)_2$). **12**: yield: 80.2%; 1H NMR (250 MHz, $CDCl_3$): $\delta = 7.79$ (d, $J = 8.3$ Hz, 2Ar-H; *o* to SO_3), 7.36 (d, $J = 8.3$ Hz, 2Ar-H; *m* to SO_3), 4.07 (d, $J = 5.5$ Hz, 2H; SO_3CH_2), 3.63–3.35 (m, 32H; OCH_2), 2.45 (s, 3H; phenyl CH_3), 2.30–2.03 (m, 1H; $OCH(OCH_2)_2$) 1.20 (t, $J = 7.0$ Hz, 18H; OCH_2CH_3).

Synthesis of 13, 14, and 15: Compounds were synthesized by using the same procedure. A representative example is described for **14**. Compound **11** (2.5 g, 3.6 mmol), 4-(hydroxymethyl)biphenyl-4′-ol (1.4 g, 6.9 mmol), and excess K_2CO_3 (≥5 equiv.) were dissolved in ethanol (50 mL). The mixture was heated at reflux for 24 h and then cooled to room temperature. The resulting solution was poured into water and extracted with methylene chloride. The solvent was removed in a rotary evaporator, and the crude mixture was purified with column chromatography (silica gel) with ethyl acetate as eluent. **13**: yield: 70.3%; 1H NMR (250 MHz, $CDCl_3$): $\delta = 7.79$–7.65 (*m*, 6Ar-H; *m* to OCH_2, *o* to CH_2OH, and *m* to CH_2OH), 6.98 (d, $J =$ 8.5 Hz, 2Ar-H; *o* to OCH_2), 4.73(s, 2H; phenyl CH_2OH), 4.11 (d, $J =$ 5.8 Hz, 2H; CH_2O phenyl), 3.65–3.51 (m, 36H; OCH_2), 3.37 (s, 12H; OCH_3), 2.43 (m, 1H; $CH(OCH_2)_2$). **14**: yield: 2.0 g (81.7%); 1H NMR (250 MHz, $CDCl_3$): $\delta = 7.79$–7.65 (*m*, 6Ar-H; *m* to OCH_2, *o* to CH_2OH, and *m* to CH_2OH), 7.00 (d, $J = 8.5$ Hz, 2Ar-H; *o* to OCH_2), 4.71(s, 2H; phenyl CH_2OH), 4.07 (d, $J = 5.8$ Hz, 2H; CH_2O phenyl), 3.64–3.43 (m, 32H; OCH_2), 3.36 (s, 12H; OCH_3), 2.32–2.03 (m, 3H; $CH(OCH_2)_2$). **15**: yield: 77.4%; 1H NMR (250 MHz, $CDCl_3$): $\delta = 7.79$–7.65 (*m*, 6Ar-H; *m* to OCH_2, *o* to CH_2OH, and *m* to CH_2OH), 7.02 (d, $J = 8.5$ Hz, 2Ar-H; *o* to OCH_2), 4.71(s, 2H; phenyl CH_2OH), 4.07 (d, $J = 5.3$ Hz, 2H; CH_2O phenyl), 3.64–3.45 (m, 32H; OCH_2), 2.25–2.10 (m, 1H, $CH(OCH_2)_2$), 1.19 (t, $J = 6.8$Hz, 18H; OCH_2CH_3).

Synthesis of 16, 17, and 18: Compounds were synthesized by using the same procedure. A representative example is described for **17**. Compound **14** (1.5 g, 2.2 mmol) and pyridinium chlorochromate (1.9 g, 8.6 mmol) were dissolved in CH_2Cl_2 (50 mL) under nitrogen. The reaction mixture was stirred at room temperature for 6 h. The CH_2Cl_2 was removed in a rotary evaporator, and the crude product was purified by column chromatography (silica gel) with diethyl ether as eluent to afford a colorless liquid. **16**: yield: 80.3%; 1H NMR (250 MHz, $CDCl_3$): $\delta = 10.04$ (s, 1H; phenyl *CH*O), 7.94 (d, $J = 8.0$ Hz, 2 Ar-H; *o* to CHO), 7.73 (d, $J = 8.0$ Hz, 2 Ar-H; *m* to CHO), 7.58 (d, $J = 8.5$ Hz, 2 Ar-H; *o* to phenyl CHO), 7.04 (d, $J = 8.5$ Hz, 2 Ar-H; *m* to phenyl CHO), 4.11 (d, $J = 5.8$ Hz, 2H; CH_2O phenyl), 3.65–3.51 (m, 36H; OCH_2), 3.37 (s, 12H; OCH_3), 2.43 (m, 1H; $CH(OCH_2)_2$). **17**: yield: 1.4 g (91.6%); 1H NMR (250 MHz, $CDCl_3$): $\delta = 10.03$ (s, 1H; phenyl *CH*O), 7.94 (d, $J = 8.0$ Hz, 2 Ar-H; *o* to CHO), 7.72 (d, $J = 8.0$ Hz, 2 Ar-H; *m* to CHO), 7.59 (d, $J = 8.5$ Hz, 2 Ar-H; *o* to phenyl CHO), 7.02 (d, $J = 8.5$ Hz, 2 Ar-H; *m* to phenyl CHO), 4.07 (d, $J = 5.8$ Hz, 2H; CH_2O phenyl), 3.64–3.43 (m, 32H; OCH_2), 3.36 (s, 12H; OCH_3), 2.32–2.03 (m, 3H; $CH(OCH_2)_2$). **18**: yield: 85.4%; 1H NMR (250 MHz, $CDCl_3$): $\delta = 10.06$ (s, 1H; phenyl *CH*O), 7.97 (d, $J = 8.3$ Hz, 2Ar-H; *o* to CHO), 7.76 (d, $J =$ 8.3 Hz, 6 Ar-H; *m* to CHO), 7.62 (d, $J = 8.3$ Hz, 2 Ar-H; *o* to phenyl CHO), 7.04 (d, $J = 8.3$ Hz, 2 Ar-H; *m* to phenyl CHO), 4.07 (d, $J = 5.3$ Hz, 2H; CH_2O phenyl), 3.64–3.45 (m, 32H; OCH_2), 2.25–2.10 (m, 1H, $CH(OCH_2)_2$), 1.19 (t, $J = 6.8$ Hz, 18H; OCH_2CH_3).

Synthesis of molecular dumbbells 1, 2, and 3: These compounds were synthesized by using the same procedure reported previously.[9] A representative example is described for **2**. Compound **17** (1.5 g, 2.1 mmol) was dissolved in dry THF (50 mL). A solution of phosphonium salt (0.15 g, 0.4 mmol) and $KOC(CH_3)_3$ (0.25 g, 2.2 mmol) in dry THF (30 mL) was added under nitrogen. The reaction mixture was stirred at room temperature under nitrogen for 24 h. The resulting solution was removed in a rotary evaporator, and the crude product was extracted with dichloromethane and water. The dichloromethane solution was washed with water, dried over anhydrous magnesium sulfate, and then filtered. The solvent was

  0947-6539/02/0804-0882 $ 17.50+.50/0 *Chem. Eur. J.* **2002**, *8*, No. 4

removed in a rotary evaporator, and the crude product was purified by column chromatography (silica gel) with a ethyl acetate/THF (8:1, *v*/*v*) as eluent to give a yellow green solid. **1**: yield: 56.6 %; 1H NMR (250 MHz, $CDCl_3$): $\delta = 7.85-7.53$ (m, 20 Ar-H; *o* to phenyl CH, *m* to phenyl CH, and *m* to OCH_2), 7.19 (s, 4 H; phenyl CH), 7.00 (d, $J = 8.8$ Hz, 4 Ar-H; o to OCH_2), 4.07 (d, $J = 5.5$ Hz, 4 H; CH_2O phenyl), 3.66–3.45 (m, 72 H; OCH_2), 3.37 (s, 24 H; OCH_3), 2.25–2.10 (m, 2 H; $CH(OCH_2)_2$); 13C NMR (62.5 MHz, $CDCl_3$): $\delta = 159.2$, 140.3, 140.1, 136.9, 136.1, 133.8, 128.7, 128.3, 127.5, 127.4, 127.2, 115.3, 72.3, 71.0, 70.9, 59.4; $M_w/M_n = 1.04$ (GPC); elemental analysis calcd for $C_{84}H_{118}O_{22}$: C 68.18, H 8.04; found C 68.01, H 8.34.

2: yield: 0.8 g (48.3 %); 1H NMR (250 MHz, $CDCl_3$): $\delta = 7.85-7.53$ (m, 20 Ar-H; *o* to phenyl CH, *m* to phenyl CH, and *m* to OCH_2), 7.18 (s, 4 H; phenyl CH), 6.99 (d, $J = 8.8$ Hz, 4 Ar-H; o to OCH_2), 4.08 (d, $J = 5.5$ Hz, 4 H; CH_2O phenyl), 3.66–3.45 (m, 64 H; OCH_2), 3.37 (s, 24 H; OCH_3), 2.25–2.10 (m, 6 H; $CH(OCH_2)_2$); 13C NMR (62.5 MHz, $CDCl_3$) $\delta = 159.2$, 140.3, 140.1, 136.9, 136.1, 133.8, 128.7, 128.2, 127.5, 127.3, 127.2, 115.3, 72.3, 71.0, 70.9, 69.8, 66.6, 59.4; $M_w/M_n = 1.05$ (GPC); elemental analysis calcd for $C_{88}H_{126}O_{22}$: C 68.81, H 8.27; found C 68.82, H, 8.16.

3: yield: 50.2 %; 1H NMR (250 MHz, $CDCl_3$): $\delta = 7.83-7.52$ (m, 20 Ar-H; *o* to phenyl CH, *m* to phenyl CH, and *m* to OCH_2), 7.19 (s, 4 H; phenyl CH), 7.01 (d, $J = 8.3$ Hz, 4 Ar-H; o to OCH_2), 4.10 (d, $J = 5.3$ Hz, 4 H; CH_2O phenyl), 3.64–3.45 (m, 64 H; OCH_2), 2.24 (m, 2 H, $CH(OCH_2)_2$), 1.14 (t, $J = 7.8$ Hz, 36 H; OCH_2CH_3); 13C NMR (62.5 MHz, $CDCl_3$) $\delta = 159.3$, 140.5, 140.1, 136.9, 136.1, 133.8, 128.8, 128.2, 127.5, 127.3, 127.2, 115.2, 70.6, 69.9, 67.1, 69.6, 45.6, 40.2, 15.5; $M_w/M_n = 1.04$ (GPC); elemental analysis calcd for $C_{91}H_{131}O_{18}$: C 72.24, H 8.73; found C 72.15, H 8.43.

Acknowledgements

This work was supported by CRM-KOSEF (2001), the Korean Science and Engineering Foundation (1999-1-308-002-3) and Pohang Accelerator Laboratory, Korea. Y.S.J. and B.K.C. acknowledge the BK 21 fellowship from the Ministry of Education, Korea

[1] G. M. Whiteside, J. P. Mathias, C. T. Seto, *Science* **1991**, *254*, 1312.
[2] M. Muthukumar, C. K. Ober, E. L. Thomas, *Science* **1997**, *277*, 1225.
[3] S. I. Stupp, *Curr. Opin. Colloid Interface Sci.* **1998**, *3*, 20.
[4] a) M. Lee, B.-K. Cho, H. Kim, W.-C. Zin, *Angew. Chem.* **1998**, *110*, 661; *Angew. Chem. Int. Ed.* **1998**, *37*, 638; b) M. Lee, B.-K. Cho, H. Kim, J.-Y. Yoon, W.-C. Zin, *J. Am. Chem. Soc.* **1998**, *120*, 9168; c) M. Lee, D.-W. Lee, B.-K. Cho, J.-Y. Yoon, W.-C. Zin, *J. Am. Chem. Soc.* **1998**, *120*, 13258; d) M. Lee, B.-K. Cho, Y.-S. Kang, W.-C. Zin, *Macromolecules* **1999**, *32*, 7688; e) M. Lee, B.-K. Cho, Y.-S. Kang, W.-C. Zin, *Macromolecules* **1999**, *32*, 8531.
[5] a) M. Lee, B.-K. Cho, Y.-G. Jang, W.-C. Zin, *J. Am. Chem. Soc.* **2000**, *122*, 7449; b) M. Lee, J.-W. Kim, I.-W. Hwang, Y.-R. Kim, N.-K. Oh, W.-C. Zin, *Adv. Mater.* **2001**, *13*, 1363.
[6] M. Lee, B.-K. Cho, K.-J. Ihn, W.-K. Lee, N.-K. Oh, W.-C. Zin, *J. Am. Chem. Soc.* **2001**, *123*, 4647.
[7] a) J. L. Segura, N. Martin, *J. Mater. Chem.* **2000**, *10*, 2403; b) S. A. Jenekhe, X. L. Chen, *Science* **1999**, *283*, 372; c) G. N. Tew, M. U. Pralle, S. I. Stupp, *Angew. Chem.* **2000**, *122*, 527; *Angew. Chem. Int. Ed.* **2000**, *39*, 517; d) M. A. Hempenius, B. M. W. Langeveld-Voss, J. A. E. H. van Haare, R. A. J. Janssen, S. S. Sheiko, J. P. Spatz, M. Möller, E. W. Meijer, *J. Am. Chem. Soc.* **1998**, *120*, 2798; e) H. Wang, H. H. Wang, V. S. Urban, K. C. Littrell, P. Thiyagarajan, L. Yu, *J. Am. Chem. Soc.* **2000**, *122*, 6855; f) J. J. Apperloo, R. A. J. Janssen, P. R. L. Malenfant, J. M. J. Frechet, *Macromolecules* **2000**, *33*, 7038.
[8] a) M. Jayaraman, J. M. J. Frechet, *J. Am. Chem. Soc.* **1998**, *120*, 12996; b) A. B. Padias, H. K. Hall, Jr., D. A. Tomalia, J. R. McConnell, *J. Org. Chem.* **1987**, *52*, 5305; c) K. M. Mondanaro, W. P. Dailey, *J. Org. Chem.* **1995**, *60*, 4666.
[9] H. Meier, M. Lehmann, *Angew. Chem.* **1998**, *110*, 664; *Angew. Chem. Int. Ed.* **1998**, *37*, 643.
[10] M. Lee, B.-K. Cho, N.-K. Oh, W.-C. Zin, *Macromolecules* **2001**, *34*, 1987.
[11] a) A. Henglein, *Chem. Rev.* **1989**, *89*, 1861; b) C. B. Murray, D. J. Norris, M. G. Bawendi, *J. Am. Chem. Soc.* **1993**, *115*, 8706.
[12] a) D. T. McQuade, J. Kim, T. M. Swager, *J. Am. Chem. Soc.* **2000**, *122*, 5885; b) G. Rumbles, I. D. W. Samuel, C. J. Collison, P. F. Miller, S. C. Moratti, A. B. Holmes, *Synth. Met.* **1999**, *101*, 158.

Received: August 3, 2001 [F3467]